

When Confidence Fails: Revisiting Pseudo-Label Selection in Semi-supervised Semantic Segmentation

Pan Liu, Jinshi Liu*
 Central South University
 {pan.liu, ljs11528}@csu.edu.cn

Abstract

While significant advances exist in pseudo-label generation for semi-supervised semantic segmentation, pseudo-label selection remains understudied. Existing methods typically use fixed confidence thresholds to retain high-confidence predictions as pseudo-labels. However, these methods cannot cope with network overconfidence tendency, where correct and incorrect predictions overlap significantly in high-confidence regions, making separation challenging and amplifying model cognitive bias. Meanwhile, the direct discarding of low-confidence predictions disrupts spatial-semantic continuity, causing critical context loss. We propose Confidence Separable Learning (CSL) to address these limitations. CSL formulates pseudo-label selection as a convex optimization problem within the confidence distribution feature space, establishing sample-specific decision boundaries to distinguish reliable from unreliable predictions. Additionally, CSL introduces random masking of reliable pixels to guide the network in learning contextual relationships from low-reliability regions, thereby mitigating the adverse effects of discarding uncertain predictions. Extensive experimental results on the Pascal, Cityscapes, and COCO benchmarks show that CSL performs favorably against state-of-the-art methods. Code and model weights are available at: <https://github.com/PanLiuCSU/CSL>.

1. Introduction

Semantic segmentation is a dense prediction task involving per-pixel classification. This technique is widely applied in critical domains such as autonomous driving and medical imaging. However, fully supervised segmentation methods [6, 9, 37] often require extensive high-quality, pixel-level labeled datasets, which can be costly and resource-intensive. In light of these challenges, semi-supervised semantic segmentation [10, 13, 21] has emerged as a promising research

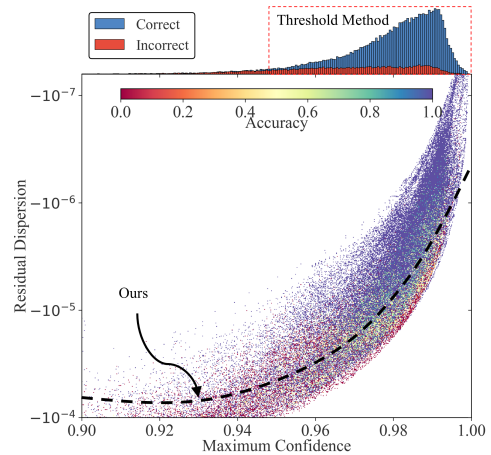


Figure 1. prediction in confidence feature space. Blue/red points and upper histogram denote correct/incorrect predictions. The threshold method (dashed box) poorly separates them, while our approach (black curve) achieves clear discrimination.

area. This approach seeks to leverage a limited number of labeled images alongside a substantial quantity of unlabeled images to improve segmentation performance.

In the field of semi-supervised semantic segmentation, combining pseudo-labeling with consistency regularization has become a popular strategy [41]. Pseudo-labeling methods [8, 26, 36, 73] generate pseudo-labels for unlabeled samples based on the model predictions to optimize the model iteratively. Consistency regularization methods [29, 40, 41, 71] follow the smoothness assumption [3], encouraging the model to generate consistent predictions under different perturbations of the same sample. The effectiveness of these strategies depends heavily on the quality of the pseudo-labels, and existing methods typically assume a direct correlation between high confidence and high accuracy, relying on the maximum confidence scores to filter or weight the pseudo-labels [23, 49, 51].

As shown by the red box in Fig. 1, neural networks often suffer from overconfidence, causing predictions to cluster at extreme confidence levels regardless of their correct-

* Corresponding author.

ness [17]. This issue becomes more pronounced when labeled data is scarce, as the limited annotations are insufficient to effectively calibrate the model’s confidence estimates on the vast unlabeled dataset. Such overconfidence presents significant challenges for semi-supervised semantic segmentation. Firstly, it renders confidence scores poor indicators of prediction accuracy, since both correct and incorrect predictions may receive similarly high confidence scores due to miscalibration. Secondly, constrained by the low distinguishability of confidence, existing methods are forced to exclude low-confidence predictions to avoid introducing errors during training [1], but this also results in a lack of supervision in borderline or complex regions of the data, that are typically crucial for model improvement.

We propose the **Confidence Separable Learning (CSL)** framework to address the challenge of insufficient discriminability of pseudo-labels. Based on entropy minimization theory, we find that reliable prediction should have both high maximum confidence and significant probability dispersion between non-maximum class probabilities. Therefore, we construct a confidence distribution feature space consisting of maximum confidence and residual deviation to guide the selection process. As shown in Fig. 1, while an overconfident network assigns similar confidence scores to correct and incorrect predictions, these two classes of predictions exhibit a high degree of separability in the confidence distribution feature space. Based on this property, CSL adaptively establishes sample-specific pseudo-label decision boundaries by formulating pseudo-label selection as a convex optimization problem that maximizes inter-class separability. This allows CSL to more adequately extract supervised signals from unlabelled data.

While CSL enhances pseudo-label reliability, its inherent precision-coverage trade-off results in the persistent exclusion of low-reliability regions from supervision, potentially amplifying regional supervision bias. To address this, we integrate a Trusted Mask Perturbation (TMP) strategy into our CSL framework. By randomly masking subsets of reliable predictions, we force the model to reconstruct semantics from adjacent unreliable regions via contextual dependencies. This process maximizes mutual information between unreliable regions and pseudo-labeled areas, thereby mitigating regional bias induced by selective pseudo-labeling. Our contributions can be summarized as:

- We demonstrate that pseudo-label selection based only on maximum confidence suffers from suboptimal performance, especially when the network is overconfident.
- We propose a semi-supervised semantic segmentation framework that separates reliable predictions by maximizing separability optimization strategy and constructs effective supervisory signals for unreliable predictions.
- Comprehensive experiments on three benchmark datasets confirm the effectiveness of our proposed method.

2. Related work

Semi-supervised learning (SSL) [27, 59, 64] aims to enhance model performance by leveraging labeled and unlabeled data. Recent investigations have concentrated on the techniques of self-training [4, 14, 42, 65, 75] and consistency regularization [30, 46, 49, 52, 66]. However, these methods limited by marginal distribution discrepancies, leading to significant erroneous supervision.

To address this limitation, two main research directions have been explored. The first focuses on optimizing threshold-based pseudo-labeling strategies [5, 61, 67, 72]. SoftMatch [5] models confidence as a Gaussian distribution to determine optimal thresholds. Despite improvements, these methods rely on assumptions that may not be universally applicable, limiting their generalizability. The second seeks additional metrics beyond confidence, such as Monte Carlo dropout [45], ensemble methods [55], and auxiliary discriminators [33]. However, the additional metrics significantly increase the computational overhead.

Semi-supervised semantic segmentation faces the challenge of generating accurate pixel-level supervisory signals for unlabeled images. Inspired by SSL, many works have adopted similar frameworks [54, 63, 70]. PS-MT [38] uses dual-teacher models to enhance consistency regularization. UniMatch [69] separates feature augmentation from image augmentation to reduce learning difficulty. Augmentation techniques like Cowmix [16] focus on providing diverse training samples.

However, these methods generally do not directly improve the quality of pseudo-labels. To overcome these limitations, several approaches have been proposed [20, 28]. AEL [23] employs a sample weighting strategy to emphasize reliable predictions. DAW [51] uses labeled data distribution to determine optimal thresholds. LOGICDIAG [34] introduces symbolic reasoning to correct erroneous pseudo-labels.

Nevertheless, these methods are still constrained by the low separability of confidence scores, resulting in biased supervisory signals. Therefore, ESL [39] uses multi-hot labels to mitigate the effects of incorrect predictions. U2PL [60] leverages unreliable predictions through contrastive learning. CorrMatch [50] utilizes correlation maps to propagate pseudo-labels in low-confidence predictions. Furthermore, this pseudo-label selection challenge exists even in unsupervised adaptation. TransCal [56] introduces calibration loss to improve the calibration performance of labelless sets. MIC [22] employing random masking strategies attempt to enhance prediction reliability. Despite these efforts, these methods face difficulties in fully eliminating inherent biases. Unlike previous approaches, CSL introduces additional metrics to address the low discriminability of confidence scores and explicitly mitigates the supervision bias caused by pseudo-labels.

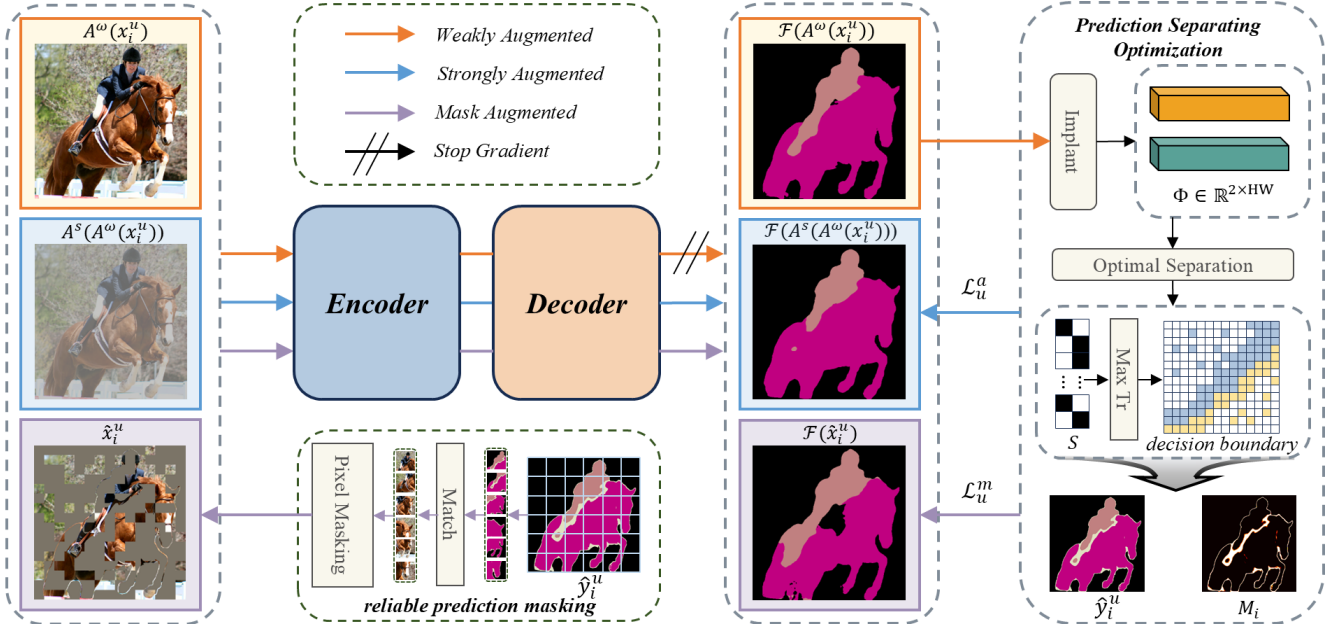


Figure 2. Overview of CSL pipeline for unlabeled images. The predictions of weakly augmented images are partitioned on a per-pixel basis into reliable and unreliable predictions through a convex optimization strategy in the feature space Φ . This process constructs loss weight mask M_i and pseudo-label \hat{y}_i^u , which are then used as supervisory signals for strongly augmented and masked images.

3. Method

3.1. Preliminaries

In semi-supervised semantic segmentation, the training data consists of a labeled set $D_l = \{(x_i^l, y_i^l)\}_{i=1}^{N_l}$ and an unlabeled set $D_u = \{x_i^u\}_{i=1}^{N_u}$, where $N_l \ll N_u$. $x_i \in \mathbb{R}^{3 \times H \times W}$ is the input image, with H and W denoting its height and width, respectively. $y_i \in \mathbb{R}^{K \times H \times W}$ is the one-hot encoded pixel label map with K classes. For the semantic segmentation network \mathcal{F} , the supervised loss is defined as:

$$\mathcal{L}_S = \frac{1}{B_L} \sum_{i=1}^{B_L} CE(y_i^l, \mathcal{F}(A^\omega(x_i^l))), \quad (1)$$

where B_L is the batch size of labeled data, $CE(\cdot, \cdot)$ denotes the cross-entropy loss function, and $A^\omega(\cdot)$ is the weak data augmentation function.

Similarly, given a batch size B_U of unlabeled data, the unsupervised training loss follows a simple framework [69] with weak-to-strong consistency regularization:

$$\mathcal{L}_u^a = \frac{1}{B_U} \sum_{i=1}^{B_U} M_i \odot CE(\hat{y}_i^u, \mathcal{F}(A^s(A^\omega(x_i^u))))), \quad (2)$$

where \hat{y}_i^u is the label derived from $F(A^\omega(x_i^u))$, $A^s(\cdot)$ is the strong data augmentation function, and M_i is the indicator mask for pseudo-labels in \hat{y}_i^u . In the baseline, following the confidence thresholding method,

$$M_i = \mathbb{I}(\max(F(A^\omega(x_i^u))) > \tau), \quad (3)$$

where $\mathbb{I}(\cdot)$ is the indicator function, τ denotes the confidence threshold. However, this strategy inevitably suffers from cognitive bias and supervision loss.

To address these issues, we propose CSL. As illustrated in Fig. 2, CSL introduces residual dispersion as an additional measure(Sec. 3.2) and through spectral relaxation, formulates M_i construction as a convex optimization problem(Sec. 3.3). Subsequently, CSL introduces additional supervisory signals that compel the network to learn global context relationships based on regions lacking supervision, compensating for supervisory gaps in challenging areas (Sec. 3.4).

3.2. Theoretical Analysis of Residual Dispersion

The overconfidence tendency of deep networks challenges the effectiveness of maximum confidence as the sole criterion for pseudo-label selection. Based on the entropy minimization principle, we theoretically demonstrate that reliable predictions should simultaneously exhibit high maximum confidence and residual dispersion.

Let $p_n \in \mathbb{R}^K$ denote the predicted class probabilities for pixel n in an unlabeled image x_i^u , $p_n(k') = \max_k p_n(k)$ represents the maximum confidence. According to entropy minimization, the ideal prediction should follow an unimodal distribution $q = [q_1, \dots, q_K]$, where $q_{k'} = 1 - (K - 1)\epsilon$ and $q_{k \neq k'} = \epsilon$ with $\epsilon \rightarrow 0$. Based on the decomposition

form of cross-entropy, the goal can be defined as

$$CE(p_n, q) = -q_{k'} \log p_n(k') - \epsilon \sum_{k \neq k'} \log p_n(k). \quad (4)$$

Decomposing non-maximum probabilities $p_n(k), \forall k \neq k'$ into mean-shift components $p_n(k) = \mu_{\text{res}} + \delta_k$, where $\mu_{\text{res}} = \frac{1-p_n(k')}{K-1}$ and $\sum_{k \neq k'} \delta_k = 0$. Applying second-order Taylor expansion to $\log p_n(k)$ around μ_{res} ,

$$\log p_n(k) = \log \mu_{\text{res}} + \frac{\delta_k}{\mu_{\text{res}}} - \frac{\delta_k^2}{2\mu_{\text{res}}^2} + \mathcal{O}(\delta_k^3), \forall k \neq k'. \quad (5)$$

Substituting Eq. (5) into Eq. (4) and simplifying,

$$CE(p_n, q) \approx -\log p_n(k') - \frac{\epsilon(K-1)^3}{2(1-p_n(k'))^2} \cdot v_n, \quad (6)$$

where the **residual dispersion** v_n is defined as

$$v_n \triangleq -\frac{1}{K-1} \sum_{k \neq k'} \delta_k^2. \quad (7)$$

Eq. (6) reveals that under entropy minimization objectives, trustworthy predictions require maximizing both maximum confidence $p_n(k')$ and residual dispersion v_n . Notably, as $p_n(k') \rightarrow 1$, the coefficient term of v_n becomes significant, shows that v_n becomes a key indicator to distinguish prediction reliability in overconfidence cases.

3.3. Prediction Convex Optimization Separation

Sec. 3.2 shows that prediction reliability nonlinearly depends on both $p_n(k')$ and v_n . However, threshold-based methods fail to capture the nonlinear complementary relationship. To overcome this limitation, we propose a sample-adaptive method, which formulates pseudo-label selection as a convex optimization problem by spectral relaxation.

We construct an attribute vector $h_n = [p_n(k'), v_n]^T$ for each pixel prediction, embedding it into a feature space that captures maximum confidence and residual dispersion. Based on this, we aim to separate predictions with high maximum confidence and residual dispersion to select reliable pseudo-labels. This selection is formalized as a trace maximization problem,

$$\max_S \text{Tr}(S^T \Phi^T \Phi S), \text{ s.t. } S \in \{0, 1\}^{HW \times 2}, \quad (8)$$

where $\text{Tr}(\cdot)$ denotes the trace of a matrix. $\Phi = [\mathbf{h}_1, \mathbf{h}_2, \dots, \mathbf{h}_{HW}]$ is the feature matrix of x_i^u . S is the selection matrix, subject to the constraint $\sum_c S_{n,c} = 1$, with $c \in \{1, 2\}$ indicates the class index in the selection.

To solve this non-convex combinatorial optimization problem, we apply spectral relaxation [43], relaxing the discrete constraints on S . According to the Ky Fan theorem [53], the optimal solution S^* approximates:

$$S_{n,c}^* = \Delta \left(\arg \max_{i \in \{1,2\}} |u_i(n)|, c \right), \quad (9)$$

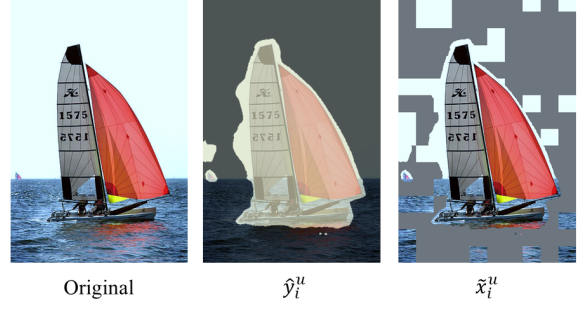


Figure 3. Illustration of Trusted Mask Perturbation. The white area in \hat{y}_i^u represents the unreliable region.

where u_1, u_2 are the eigenvectors of the matrix $\Phi^T \Phi$, $|u_i(n)|$ denotes the absolute value of the n -th element in u_i , and $\Delta(\cdot, \cdot)$ is the Kronecker delta function.

Without loss of generality, assuming that $c = 2$ indicates the subset of predictions with high maximum confidence and residual dispersion, we define the projection matrix $Z = \Phi S_{n,2}^*$, representing the projection of predictions onto the reliable component. Based on this, applying a Gaussian weighting function to construct smooth loss weights ω_n ,

$$\omega_n = \prod_c \exp \left(\frac{(h_n(c) - \mu_c)^2}{-\alpha \sigma_c^2} \right), \quad (10)$$

where μ_c is the mean of the high-reliability prediction subset in the projection matrix Z for component c , and σ_c is its variance. $\alpha = 8$ is the smoothing parameter. To ensure that predictions with high maximum confidence and residual dispersion are always retained, the weights of these predictions are set to 1. Therefore, the unsupervised training indicator mapping M_i for x_i^u is defined as:

$$M_i(n) = \begin{cases} 1 & \text{if } (h_n(c) - \mu_c) > 0, \forall c \in \{1, 2\} \\ \omega_n & \text{otherwise} \end{cases}. \quad (11)$$

3.4. Trusted Mask Perturbation

While semi-supervised training can benefit from high-quality pseudo-labels, persistent exclusion of challenging regions risks entrenching the model in simplistic patterns. To mitigate this, we propose the Trusted Mask Perturbation (TMP), which selectively masks high-confidence predictions, thereby implicitly supervising unreliable regions using contextual information.

Utilizing the reliable pixel indicator M_i from Sec. 3.3, where $M_i = 1$ denotes reliable predictions, we define a patch-based perturbation mask $R_i \in \{0, 1\}^{H \times W}$ generated as follows:

$$R_i(x, y) = \mathbb{I}(M_i(x, y) = 1) \cdot \mathbb{I}(U(\lfloor \frac{x}{s} \rfloor, \lfloor \frac{y}{s} \rfloor) \geq \theta), \quad (12)$$

PASCAL <i>original</i>	Train Size	1/16(92)	1/8(183)	1/4(366)	1/2(732)	Full(1464)
Supervised	321 × 321	45.4	53.1	61.2	68.4	73.2
ST++ [68]	321 × 321	65.2	71.0	74.6	77.3	79.1
UniMatch [69]	321 × 321	75.2	77.2	78.8	79.9	81.2
CorrMatch [50]	321 × 321	76.4	78.5	79.4	80.6	81.8
ESL [39]	513 × 513	71.0	74.1	78.1	79.5	81.8
LogicDiag [34]	513 × 513	73.3	76.7	78.0	79.4	-
RankMatch [40]	513 × 513	75.5	77.6	79.8	80.7	82.2
AugSeg [74]	513 × 513	71.1	75.5	78.8	80.3	81.4
SemiCVT [24]	513 × 513	68.6	71.3	75.0	78.5	80.3
FPL [44]	513 × 513	69.3	71.7	75.7	79.0	-
AllSpark [54]	513 × 513	76.1	78.4	79.8	80.8	82.1
CSL	321 × 321	76.8	79.6	80.3	80.9	82.3

Table 1. Comparison with SOTAs on the PASCAL VOC 2012 original dataset under different splits. All labelled images were selected from the original VOC training set, which consists of 1,464 images. The fractions denote the percentage of labeled data used for training.

where $s = 32$ is the patch size, $\theta = 0.7$ is the masking ratio, and $U(\cdot, \cdot)$ denotes the uniform distribution over the interval $[0, 1]$.

The perturbed image \tilde{x}_i^u is obtained by applying R_i to the input image x_i^u :

$$\tilde{x}_i^u = x_i^u \odot R_i, \quad (13)$$

where \odot denotes element-wise multiplication. As illustrated in Fig. 3, this strategy selectively masks reliable pixels, compelling the model to infer the missing content based on contextual cues from the remaining challenging regions.

The unsupervised loss for the masked inputs is formulated as:

$$\mathcal{L}_u^m = \frac{1}{B_U} \sum_{i=1}^{B_U} M_i \odot CE(\hat{y}_i^u, F(\tilde{x}_i^u)). \quad (14)$$

The final unsupervised loss term combines both the standard and masked losses:

$$\mathcal{L}_U = \lambda_1 L_u^a + \lambda_2 L_u^m, \quad (15)$$

where λ_1, λ_2 are loss weights set to $[0.5, 0.5]$ by default.

4. Experiments

4.1. Implementation Details

Datasets. We evaluate the proposed method on three benchmark datasets: PASCAL VOC 2012, Cityscapes, and MS COCO. PASCAL VOC 2012 [15] is a standard semantic segmentation dataset comprising 20 object classes and one background class. The training and validation sets contain 1,464 and 1,449 images, respectively. Following previous works [25, 76], we augment the training set by incorporating 9,118 images with coarse annotations from the Segmentation Boundary Dataset (SBD) [18], resulting in a blender

set of 10,582 training images. Cityscapes [12] focuses on urban scene understanding and includes 19 classes. It consists of 2,975 finely annotated training images and 500 validation images, all at a high resolution of 1024×2048. MS COCO [35] is a large-scale dataset with 81 object categories, containing 118k training and 5k validation images for segmentation tasks.

Implementation Details. To ensure a fair comparison with prior methods, we adopt the ResNet [19] backbone with DeepLabv3+ [7] as the decoder for PASCAL VOC 2012 and Cityscapes, and Xception-65 [11] for MS COCO [35]. For all datasets, we use SGD with a batch size of 8 and weight decay of 1×10^{-4} . For PASCAL VOC 2012, we set the initial learning rate to 0.001, crop size of 321×321 or 513×513, training epochs of 80, and a decoder learning rate ten times that of the backbone. For Cityscapes, we use an initial learning rate of 0.001, crop size of 801×801, and training epochs of 240, with OHEM [48]. For COCO, we set the initial learning rate to 0.004, crop size of 513×513 and train for 30 epochs.

Evaluation Metrics. For PASCAL VOC 2012, we follow standard protocols [20, 60], reporting mIoU on the original validation images. For Cityscapes, we perform sliding window evaluation with a crop size of 801×801 and compute mIoU [23, 31]. For COCO, we evaluate on the standard 5k validation set with mIoU. Ablation studies are conducted on PASCAL VOC 2012 with a crop size of 321×321.

4.2. Comparison with State-of-the-Art Methods

Original PASCAL VOC 2012. Tab. 1 presents the comparison results on the original PASCAL VOC 2012 dataset. Compared to the supervised baseline, CSL consistently achieves significant performance improvements. Specifically, under the 1/16, 1/8, 1/4, 1/2, and full data splits, CSL attains improvements of +31.4%, +26.5%, +19.1%,

PASCAL blender	Train Size	1/16 (662)	1/8 (1323)	1/4 (2646)
ST++ [68]	321 × 321	74.5	76.3	76.6
UniMatch [69]	321 × 321	76.5	77.0	77.2
CorrMatch [50]	321 × 321	<u>77.6</u>	<u>77.8</u>	<u>78.3</u>
CAC [29]	321 × 321	72.4	74.6	76.3
CSL	321 × 321	77.8	78.5	79.0
U2PL [†] [60]	513 × 513	77.2	79.0	79.3
GTA [†] [25]	513 × 513	77.8	80.4	80.5
CorrMatch [†] [50]	513 × 513	81.3	81.9	<u>80.9</u>
UniMatch [†] [69]	513 × 513	81.0	81.9	80.4
AugSeg [†] [74]	513 × 513	79.3	81.5	80.5
AllSpark [†] [54]	513 × 513	<u>81.6</u>	<u>82.0</u>	80.9
CSL[†]	513 × 513	81.6	82.4	81.1

Table 2. Comparison with SOTAs on PASCAL VOC 2012 blender dataset. All labelled images were selected from the blender VOC training set under different splits, which consists of 10,582 images. [†] means using U2PL’s splits.

Cityscapes	1/16(186)	1/8(732)	1/4(744)	1/2(1488)
Supervised	63.1	70.5	73.1	76.2
ST++ [68]	67.6	73.4	74.6	77.8
UniMatch [69]	76.6	77.9	79.2	79.5
CorrMatch [50]	<u>77.3</u>	78.5	79.4	80.4
ESL [39]	75.1	77.2	79.0	80.5
DGCL [57]	73.2	77.3	78.5	80.7
AugSeg [74]	75.2	77.8	79.6	80.4
CCVC [62]	74.9	76.4	77.3	-
DAW [51]	76.6	78.4	79.8	80.6
U2PL [60]	70.3	74.4	76.5	79.1
CPS [8]	69.8	74.3	74.6	76.8
DDFP [58]	77.1	78.2	<u>79.9</u>	<u>80.8</u>
FPL [44]	75.7	<u>78.5</u>	79.2	-
CSL	78.2	78.8	80.0	81.1

Table 3. Comparison with SOTAs on Cityscapes dataset. All methods are built upon DeepLabV3+ [7] and ResNet101 [19].

+12.5%, and +9.1%, respectively. Moreover, when compared with existing SOTAs, our approach consistently demonstrates superior performance. Particularly, under the 1/8 and 1/4 splits, CSL outperforms UniMatch [69] by +2.4% and +1.5%, respectively.

Blender PASCAL VOC 2012. We show the comparison between our method and SOTAs on the blender PASCAL VOC 2012 dataset in Tab. 2. At a crop size of 321×321, CSL surpasses CorrMatch [50] by +0.2%, +0.7%, and +0.7%. We observe that the performance gains become more pronounced as the amount of available annotations decreases. For instance, at a crop size of 513×513 under the 1/16 splits,

PASCAL blender	Train Size	1/16 (662)	1/8 (1323)	1/4 (2646)
ST++ [68]	513 × 513	74.7	77.9	77.9
UniMatch [69]	513 × 513	78.1	78.4	79.2
CorrMatch [50]	513 × 513	78.4	79.3	79.6
ESL [39]	513 × 513	76.4	78.6	79.0
PS-MT [38]	513 × 513	75.5	78.2	78.7
CFCG [32]	513 × 513	76.8	79.1	80.0
CCVC [62]	513 × 513	77.2	78.4	79.0
DLG [31]	513 × 513	77.8	79.3	79.1
RankMatch [40]	513 × 513	<u>78.9</u>	79.2	80.0
DGCL [57]	513 × 513	76.6	78.3	79.3
AllSpark [54]	513 × 513	78.3	80.0	80.4
DDFP [58]	513 × 513	78.3	78.9	79.8
CSL	513 × 513	78.9	<u>79.9</u>	<u>80.3</u>

COCO	1/512	1/256	1/128	1/64	1/32
Supervised	22.5	28.3	33.1	38.9	42.1
UniMatch [69]	31.9	38.9	44.4	48.2	49.8
LogicDiag [34]	<u>33.1</u>	<u>40.3</u>	<u>45.4</u>	<u>48.8</u>	<u>50.5</u>
PseudoSeg [76]	29.8	37.1	39.1	41.8	43.6
CSL	35.1	42.3	45.8	49.7	51.2

Table 4. Comparison with SOTAs on MS-COCO dataset. All methods are built upon XC-65 [11] for fair comparison.

our method improves upon AllSpark [54] by +0.6%.

Additionally, we conduct experiments using the same splits as U2PL [60], where the supervised dataset primarily consists of high-quality annotations supplemented with a small amount of coarse annotation data. Under the 1/8 splits, since most high-quality annotations are included and the coarse annotations are largely excluded, the model benefits from a robust initial representation. This enables our method to achieve an outstanding performance of 82.4%, representing a +0.9% improvement over AugSeg [74]. This significant performance gain demonstrates our method’s ability to effectively leverage accurate network representations in scenarios with scarce annotations.

Cityscapes. Tab. 3 quantitatively compares the performance of CSL with SOTAs on the Cityscapes validation set. Leveraging the extensive unlabeled data, CSL achieves performance gains of +15.1%, +8.3%, +6.9%, and +5.1% over the supervised baseline under the 1/16, 1/8, 1/4, and 1/2 splits, respectively. CSL surpasses existing SOTAs across all partition protocols. For example, under the 1/16 partition, our method achieves a +0.9% performance improvement over CorrMatch [50].

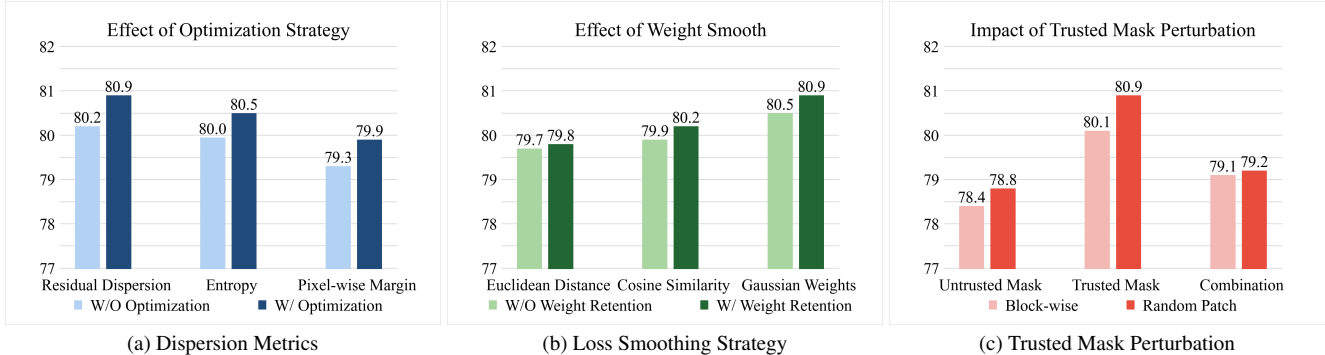


Figure 4. Ablation studies on different designs of CSL. For (a), (b), and (c), experiments are conducted on the 1/2 splits.

SemiBaseline	M_i	CSL ω_n	\mathcal{L}_u^m	1/16 (92)	1/2 (732)
✓				72.9	78.6
✓	✓			73.8	79.3
✓	✓	✓		74.2	79.8
✓			✓	73.6	79.4
✓	✓	✓	✓	76.8	80.9

Table 5. Ablation study on the effectiveness of different components, including optimization strategy M_i , smooth loss weight ω_n , trusted mask perturbation \mathcal{L}_u^m .

MS COCO. Tab. 4 presents the quantitative comparisons of CSL with SOTAs on the MS COCO dataset. Across all partition ratios, CSL consistently outperforms existing approaches by significant margins. Notably, when utilizing only 1/512 of the labeled data, CSL achieves an impressive 35.1% mIoU, surpassing the strongest baseline Logic-Diag [34] by +2.0%.

4.3. Ablation Studies

Effectiveness of components. We conducted ablation studies on the different components of CSL to demonstrate their effectiveness, as shown in Tab. 5. Starting with a semi-supervised baseline, we achieve mIoU scores of 72.9% and 78.6% for the 1/16 and 1/2 splits, respectively. By introducing the residual dispersion and optimization strategy M_i , the performance improves to 73.8% and 79.3%. Building upon this, incorporating the smooth loss weight ω_n yields additional gains of 0.4% and 0.5%. By combining all components, our method surpasses the baseline by over 3.9% and 2.3%, achieving SOTA results. Notably, adding the trusted mask perturbation \mathcal{L}_u^m alone to the semi-supervised baseline results in performance gains of 0.7% and 0.8%, illustrating its general applicability in addressing the lack of supervision in challenging regions of pseudo-labels.

Evaluation of Dispersion Metrics. Fig. 4a compares resid-

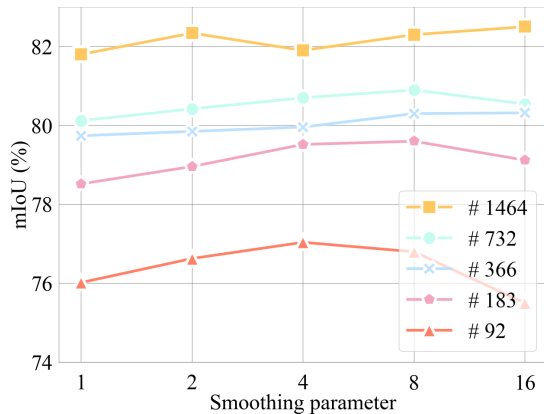


Figure 5. Ablation study of smoothing parameter α .

ual dispersion with pixel-wise margin [47] and entropy. Both margin and entropy exhibit significant performance degradation. Because when the model is overconfident, the margin dominates by the maximum confidence, while entropy becomes insensitive to non-maximum confidence values. Under such circumstances, reliability assessment degenerates into merely comparing maximum confidence scores. Following the setup in Sec. 3.2, residual dispersion maintains magnitude consistency in scale and coefficients, ensuring robust pseudo-label selection. Meanwhile, replacing the optimization strategy with sample-wise mean thresholds [5] resulted in consistent performance degradation, validating the necessity of our design.

Weight smoothing strategy. CSL constructs smoothed loss weights by the Gaussian weighting function. We compare it with alternative measures, including Euclidean distance and cosine similarity. Additionally, we examined the effect of retaining loss weights for reliable predictions versus uniformly smoothing all loss weights. As shown in Fig. 4b, combining Gaussian weighting with retention of reliable prediction loss weights yields the most significant performance improvement. Suggests that our approach ensures

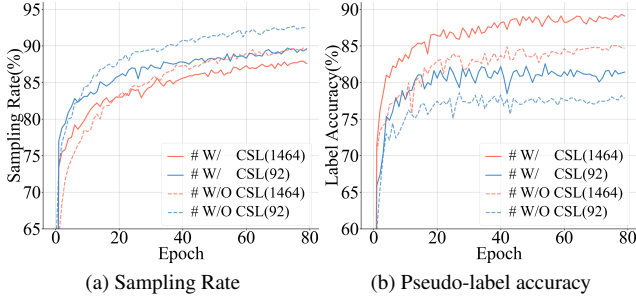


Figure 6. Training curves for our CSL and the threshold strategy.

Patch Size s	8	16	32	64
$\theta=0.3$	78.7	78.5	78.4	76.2
$\theta=0.5$	78.2	79.1	78.9	77.8
$\theta=0.7$	78.8	79.2	79.4	78.4
$\theta=0.9$	77.5	77.6	77.6	77.4

Table 6. Ablation study with different mask perturbation parameters for 1/2 splits.

models learn effectively from credible examples, enhancing overall segmentation performance.

Impact of trusted mask perturbation. Fig. 4c analyses the performance of block-wise masking [2] versus random patch masking across different masking targets. The results show that masking only reliable predictions yields the best performance. In contrast, masking untrustworthy predictions or both results in significant performance degradation. This decline may stem from the absence of supervised signals and image content in untrustworthy regions, leading to excessive perturbation. Furthermore, random patch masking consistently outperforms block-wise masking due to the increased sample diversity introduced.

Impact of hyperparameters. The effects of the loss smoothing coefficient α , masking patch size s , and masking rate θ on the PASCAL VOC 2012 dataset were investigated. Fig. 5 illustrates that an excessively high value of α leads to performance degradation, which results from the improper weighting of unreliable predictions. Consequently, $\alpha = 8$ has been established as the default value to optimize overall performance. Tab. 6 demonstrates that optimal performance enhancement is achieved from credible masking when $\theta = 0.7$ and $s = 32$. In contrast, when the masking patch size $s = 64$, the mIoU decreases significantly, which is attributed to the extreme size of the patch compared to the image size, ultimately leading to a loss of local contextual information.

4.4. Qualitative analysis

CSL improved semi-supervised training. To evaluate the effectiveness of CSL, we measured the average accuracy and the average sampling rate of pseudo-labels produced by



Figure 7. Qualitative results on the PASCAL VOC 2012 dataset. (a) Pseudo labels without CSL; (b) Pseudo labels with CSL; (c) Ground truth.

our method and threshold-based methods. As seen in Fig. 6, suffering from overconfidence, as the quantity of labeled data diminishes, threshold-based methods exhibit a proclivity for increasingly assertive pseudo-label selection, resulting in a notable surge in false supervision signals. In contrast, CSL demonstrates superior performance in mitigating cognitive biases and consistently generates high-quality pseudo-labels.

Qualitative Results. Fig. 7 illustrates the visualization results for the PASCAL VOC 2012 dataset under 1/8 splits. Obviously, our predictive convex optimized segmentation strategy effectively broadens the regions encompassed by pseudo-labels. By utilizing plausible mask perturbations, CSL achieves more accurate and detailed segmentation in intricate areas, and the visualization results demonstrate its capacity to enhance segmentation performance by leveraging unlabelled data and addressing supervision gaps.

5. Conclusions

We demonstrate that through comprehensive measurement of maximum confidence and residual dispersion, a pronounced natural separation exists between reliable predictions and cognitive biases. Motivated by this, we explore pseudo-label selection in this space through a convex optimization strategy. On the other hand, we attempt to motivate the supervised signals of reliable predictions to improve prediction results in unreliable regions by masking the reliable pixels. Experiments demonstrate the significant effectiveness of decision boundaries in this space, and that masking strategy significantly improves prediction results in complex regions. In addition, comparative experiments demonstrate the superiority of CSL over other methods.

Acknowledgements. This work is supported by the China Postdoctoral Program for State-Owned Enterprises (GZC20251179) and Hunan Youth Science Foundation Program (2025JJ60424).

References

- [1] Eric Arazo, Diego Ortego, Paul Albert, Noel E O’Connor, and Kevin McGuinness. Pseudo-labeling and confirmation bias in deep semi-supervised learning. In *IJCNN*, pages 1–8. IEEE, 2020. 2
- [2] Hangbo Bao, Li Dong, Songhao Piao, and Furu Wei. Beit: Bert pre-training of image transformers. In *ICLR*, 2021. 8
- [3] Olivier Chapelle, Bernhard Scholkopf, and Alexander Zien. Semi-supervised learning. *IEEE Transactions on Neural Networks*, 20(3):542–542, 2009. 1
- [4] Baixu Chen, Junguang Jiang, Ximei Wang, Pengfei Wan, Jianmin Wang, and Mingsheng Long. Debaised self-training for semi-supervised learning. *NeurIPS*, 35:32424–32437, 2022. 2
- [5] Hao Chen, Ran Tao, Yue Fan, Yidong Wang, Jindong Wang, Bernt Schiele, Xing Xie, Bhiksha Raj, and Marios Savvides. Softmatch: Addressing the quantity-quality tradeoff in semi-supervised learning. In *ICLR*, 2023. 2, 7
- [6] Liang-Chieh Chen, George Papandreou, Iasonas Kokkinos, Kevin Murphy, and Alan L Yuille. Deeplab: Semantic image segmentation with deep convolutional nets, atrous convolution, and fully connected crfs. *IEEE TPAMI*, 40(4):834–848, 2017. 1
- [7] Liang-Chieh Chen, Yukun Zhu, George Papandreou, Florian Schroff, and Hartwig Adam. Encoder-decoder with atrous separable convolution for semantic image segmentation. In *ECCV*, pages 801–818, 2018. 5, 6
- [8] Xiaokang Chen, Yuhui Yuan, Gang Zeng, and Jingdong Wang. Semi-supervised semantic segmentation with cross pseudo supervision. In *CVPR*, pages 2613–2622, 2021. 1, 6
- [9] Xinyue Chen, Miaoqing Shi, Zijian Zhou, Lianghua He, and Sophia Tsoka. Enhancing generalized few-shot semantic segmentation via effective knowledge transfer. In *AAAI*, 2025. 1
- [10] Shengyang Cheng, Jianyong Huang, Xiaodong Wang, Lei Huang, and Zhiqiang Wei. Image-text aggregation for open-vocabulary semantic segmentation. *Neurocomputing*, page 129702, 2025. 1
- [11] François Chollet. Xception: Deep learning with depthwise separable convolutions. In *CVPR*, pages 1251–1258, 2017. 5, 6
- [12] Marius Cordts, Mohamed Omran, Sebastian Ramos, Timo Rehfeld, Markus Enzweiler, Rodrigo Benenson, Uwe Franke, Stefan Roth, and Bernt Schiele. The cityscapes dataset for semantic urban scene understanding. In *CVPR*, pages 3213–3223, 2016. 5
- [13] Jiacheng Deng, Jiahao Lu, and Tianzhu Zhang. Quantity-quality enhanced self-training network for weakly supervised point cloud semantic segmentation. *IEEE TPAMI*, 2025. 1
- [14] Ye Du, Yujun Shen, Haochen Wang, Jingjing Fei, Wei Li, Liwei Wu, Rui Zhao, Zehua Fu, and Qingjie Liu. Learning from future: A novel self-training framework for semantic segmentation. *NeurIPS*, 35:4749–4761, 2022. 2
- [15] Mark Everingham, SM Ali Eslami, Luc Van Gool, Christopher KI Williams, John Winn, and Andrew Zisserman. The pascal visual object classes challenge: A retrospective. *IJCV*, 111:98–136, 2015. 5
- [16] G. French, S. Laine, T. Aila, and M. Mackiewicz. Semi-supervised semantic segmentation needs strong, varied perturbations. In *BMVC*, 2020. 2
- [17] Chuan Guo, Geoff Pleiss, Yu Sun, and Kilian Q Weinberger. On calibration of modern neural networks. In *ICML*, pages 1321–1330. PMLR, 2017. 2
- [18] Bharath Hariharan, Pablo Arbeláez, Lubomir Bourdev, Subhransu Maji, and Jitendra Malik. Semantic contours from inverse detectors. In *ICCV*, pages 991–998, 2011. 5
- [19] Kaiming He, Xiangyu Zhang, Shaoqing Ren, and Jian Sun. Deep residual learning for image recognition. In *CVPR*, pages 770–778, 2016. 5, 6
- [20] Ruifei He, Jihan Yang, and Xiaojuan Qi. Re-distributing biased pseudo labels for semi-supervised semantic segmentation: A baseline investigation. In *CVPR*, pages 6930–6940, 2021. 2, 5
- [21] Seunghoon Hong, Hyeonwoo Noh, and Bohyung Han. Decoupled deep neural network for semi-supervised semantic segmentation. *NeurIPS*, 28, 2015. 1
- [22] Lukas Hoyer, Dengxin Dai, Haoran Wang, and Luc Van Gool. Mic: Masked image consistency for context-enhanced domain adaptation. In *CVPR*, pages 11721–11732, 2023. 2
- [23] Hanzhe Hu, Fangyun Wei, Han Hu, Qiwei Ye, Jinshi Cui, and Liwei Wang. Semi-supervised semantic segmentation via adaptive equalization learning. *NeurIPS*, 34:22106–22118, 2021. 1, 2, 5
- [24] Huimin Huang, Shiao Xie, Lanfen Lin, Ruofeng Tong, Yen-Wei Chen, Yuexiang Li, Hong Wang, Yawen Huang, and Yefeng Zheng. Semicvt: Semi-supervised convolutional vision transformer for semantic segmentation. In *CVPR*, pages 11340–11349, 2023. 5
- [25] Ying Jin, Jiaqi Wang, and Dahua Lin. Semi-supervised semantic segmentation via gentle teaching assistant. *NeurIPS*, 35:2803–2816, 2022. 5, 6
- [26] Rihuan Ke, Angelica I Aviles-Rivero, Saurabh Pandey, Saikumar Reddy, and Carola-Bibiane Schönlieb. A three-stage self-training framework for semi-supervised semantic segmentation. *IEEE TIP*, 31:1805–1815, 2022. 1
- [27] Jiwon Kim, Youngjo Min, Daehwan Kim, Gyuseong Lee, Junyoung Seo, Kwangrok Ryoo, and Seungryong Kim. Con-match: Semi-supervised learning with confidence-guided consistency regularization. In *ECCV*, pages 674–690. Springer, 2022. 2
- [28] Donghyeon Kwon and Suha Kwak. Semi-supervised semantic segmentation with error localization network. In *CVPR*, pages 9957–9967, 2022. 2
- [29] Xin Lai, Zhuotao Tian, Li Jiang, Shu Liu, Hengshuang Zhao, Liwei Wang, and Jiaya Jia. Semi-supervised seman-

- tic segmentation with directional context-aware consistency. In *CVPR*, pages 1205–1214, 2021. 1, 6
- [30] Samuli Laine and Timo Aila. Temporal ensembling for semi-supervised learning. *arXiv preprint arXiv:1610.02242*, 2016. 2
- [31] Peixia Li, Pulak Purkait, Thalaiyasingam Ajanthan, Majid Abdolshah, Ravi Garg, Hisham Husain, Chenchen Xu, Stephen Gould, Wanli Ouyang, and Anton Van Den Hengel. Semi-supervised semantic segmentation under label noise via diverse learning groups. In *CVPR*, pages 1229–1238, 2023. 5, 6
- [32] Shuo Li, Yue He, Weiming Zhang, Wei Zhang, Xiao Tan, Junyu Han, Errui Ding, and Jingdong Wang. Cfcg: Semi-supervised semantic segmentation via cross-fusion and contour guidance supervision. In *CVPR*, pages 16348–16358, 2023. 6
- [33] Siyuan Li, Weiyang Jin, Zedong Wang, Fang Wu, Zicheng Liu, Cheng Tan, and Stan Z Li. Semireward: A general reward model for semi-supervised learning. In *ICLR*, 2024. 2
- [34] Chen Liang, Wenguan Wang, Jiaxu Miao, and Yi Yang. Logic-induced diagnostic reasoning for semi-supervised semantic segmentation. In *CVPR*, pages 16197–16208, 2023. 2, 5, 6, 7, 13
- [35] Tsung-Yi Lin, Michael Maire, Serge Belongie, James Hays, Pietro Perona, Deva Ramanan, Piotr Dollár, and C Lawrence Zitnick. Microsoft coco: Common objects in context. In *ECCV*, pages 740–755. Springer, 2014. 5
- [36] Jinshi Liu, Zhaohui Jiang, Ting Cao, Zhiwen Chen, Chaobo Zhang, and Weihua Gui. Generated pseudo-labels guided by background skeletons for overcoming under-segmentation in overlapping particle objects. *TCSVT*, 33(6):2906–2919, 2022. 1
- [37] Jinshi Liu, Zhaohui Jiang, Weihua Gui, Zhiwen Chen, and Chaobo Zhang. Occlusion segmentation: Restore and segment invisible areas for particle objects. *IEEE Transactions on Automation Science and Engineering*, 2024. 1
- [38] Yuyuan Liu, Yu Tian, Yuanhong Chen, Fengbei Liu, Vasileios Belagiannis, and Gustavo Carneiro. Perturbed and strict mean teachers for semi-supervised semantic segmentation. In *CVPR*, pages 4258–4267, 2022. 2, 6
- [39] Jie Ma, Chuan Wang, Yang Liu, Liang Lin, and Guanbin Li. Enhanced soft label for semi-supervised semantic segmentation. In *CVPR*, pages 1185–1195, 2023. 2, 5, 6
- [40] Huayu Mai, Rui Sun, Tianzhu Zhang, and Feng Wu. Rankmatch: Exploring the better consistency regularization for semi-supervised semantic segmentation. In *CVPR*, pages 3391–3401, 2024. 1, 5, 6
- [41] Sudhanshu Mittal, Maxim Tatarchenko, and Thomas Brox. Semi-supervised semantic segmentation with high-and low-level consistency. *IEEE TPAMI*, 43(4):1369–1379, 2019. 1
- [42] Takeru Miyato, Shin-ichi Maeda, Masanori Koyama, and Shin Ishii. Virtual adversarial training: a regularization method for supervised and semi-supervised learning. *IEEE TPAMI*, 41(8):1979–1993, 2018. 2
- [43] Carl Olsson, Anders P Eriksson, and Fredrik Kahl. Improved spectral relaxation methods for binary quadratic optimization problems. *Computer Vision and Image Understanding*, 112(1):3–13, 2008. 4
- [44] Pengchong Qiao, Zhidan Wei, Yu Wang, Zhennan Wang, Guoli Song, Fan Xu, Xiangyang Ji, Chang Liu, and Jie Chen. Fuzzy positive learning for semi-supervised semantic segmentation. In *CVPR*, pages 15465–15474, 2023. 5, 6
- [45] Mamshad Nayeem Rizve, Kevin Duarte, Yogesh S Rawat, and Mubarak Shah. In defense of pseudo-labeling: An uncertainty-aware pseudo-label selection framework for semi-supervised learning. *arXiv preprint arXiv:2101.06329*, 2021. 2
- [46] Mehdi Sajjadi, Mehran Javanmardi, and Tolga Tasdizen. Regularization with stochastic transformations and perturbations for deep semi-supervised learning. *NeurIPS*, 29, 2016. 2
- [47] Gyungin Shin, Weidi Xie, and Samuel Albanie. All you need are a few pixels: semantic segmentation with pixelpick. In *ICCV*, pages 1687–1697, 2021. 7
- [48] Abhinav Shrivastava, Abhinav Gupta, and Ross Girshick. Training region-based object detectors with online hard example mining. In *CVPR*, pages 761–769, 2016. 5
- [49] Kihyuk Sohn, David Berthelot, Nicholas Carlini, Zizhao Zhang, Han Zhang, Colin A Raffel, Ekin Dogus Cubuk, Alexey Kurakin, and Chun-Liang Li. Fixmatch: Simplifying semi-supervised learning with consistency and confidence. *NeurIPS*, 33:596–608, 2020. 1, 2
- [50] Boyuan Sun, Yuqi Yang, Le Zhang, Ming-Ming Cheng, and Qibin Hou. Corrmatch: Label propagation via correlation matching for semi-supervised semantic segmentation. In *CVPR*, pages 3097–3107, 2024. 2, 5, 6, 13
- [51] Rui Sun, Huayu Mai, Tianzhu Zhang, and Feng Wu. Daw: exploring the better weighting function for semi-supervised semantic segmentation. *NeurIPS*, 36, 2024. 1, 2, 6, 13
- [52] Antti Tarvainen and Harri Valpola. Mean teachers are better role models: Weight-averaged consistency targets improve semi-supervised deep learning results. *NeurIPS*, 30, 2017. 2
- [53] GQ Tian. Generalized kkm theorems, minimax inequalities, and their applications. *Journal of Optimization Theory and Applications*, 83:375–389, 1994. 4
- [54] Haonan Wang, Qixiang Zhang, Yi Li, and Xiaomeng Li. Allspark: Reborn labeled features from unlabeled in transformer for semi-supervised semantic segmentation. In *CVPR*, pages 3627–3636, 2024. 2, 5, 6, 14
- [55] Kuo Wang, Yuxiang Nie, Chaowei Fang, Chengzhi Han, Xuewen Wu, Xiaohui Wang, Liang Lin, Fan Zhou, and Guanbin Li. Double-check soft teacher for semi-supervised object detection. In *IJCAI*, pages 1430–1436, 2022. 2
- [56] Ximei Wang, Mingsheng Long, Jianmin Wang, and Michael Jordan. Transferable calibration with lower bias and variance in domain adaptation. *Advances in Neural Information Processing Systems*, 33:19212–19223, 2020. 2
- [57] Xiaoyang Wang, Bingfeng Zhang, Limin Yu, and Jimin Xiao. Hunting sparsity: Density-guided contrastive learning for semi-supervised semantic segmentation. In *CVPR*, pages 3114–3123, 2023. 6
- [58] Xiaoyang Wang, Huihui Bai, Limin Yu, Yao Zhao, and Jimin Xiao. Towards the uncharted: Density-descending feature perturbation for semi-supervised semantic segmentation. In *CVPR*, pages 3303–3312, 2024. 6

- [59] Yidong Wang, Hao Chen, Yue Fan, Wang Sun, Ran Tao, Wenxin Hou, Renjie Wang, Linyi Yang, Zhi Zhou, Lan-Zhe Guo, et al. Usb: A unified semi-supervised learning benchmark for classification. *NeurIPS*, 35:3938–3961, 2022. 2
- [60] Yuchao Wang, Haochen Wang, Yujun Shen, Jingjing Fei, Wei Li, Guoqiang Jin, Liwei Wu, Rui Zhao, and Xinyi Le. Semi-supervised semantic segmentation using unreliable pseudo-labels. In *CVPR*, pages 4248–4257, 2022. 2, 5, 6
- [61] Yidong Wang, Hao Chen, Qiang Heng, Wenxin Hou, Yue Fan, Zhen Wu, Jindong Wang, Marios Savvides, Takahiro Shinozaki, Bhiksha Raj, et al. Freematch: Self-adaptive thresholding for semi-supervised learning. In *ICLR*, 2023. 2
- [62] Zicheng Wang, Zhen Zhao, Xiaoxia Xing, Dong Xu, Xiangyu Kong, and Luping Zhou. Conflict-based cross-view consistency for semi-supervised semantic segmentation. In *CVPR*, pages 19585–19595, 2023. 6
- [63] Zhenyan Wang, Zhenxue Chen, Chengyun Liu, Yaping Zhao, Xinming Zhu, and QM Jonathan Wu. Diversity augmentation and multi-fuzzy label for semi-supervised semantic segmentation. *Neurocomputing*, page 129681, 2025. 2
- [64] Qizhe Xie, Zihang Dai, Eduard Hovy, Thang Luong, and Quoc Le. Unsupervised data augmentation for consistency training. *NeurIPS*, 33:6256–6268, 2020. 2
- [65] Qizhe Xie, Minh-Thang Luong, Eduard Hovy, and Quoc V Le. Self-training with noisy student improves imagenet classification. In *CVPR*, pages 10687–10698, 2020. 2
- [66] Haiming Xu, Lingqiao Liu, Qiuchen Bian, and Zhen Yang. Semi-supervised semantic segmentation with prototype-based consistency regularization. *NeurIPS*, 35:26007–26020, 2022. 2
- [67] Yi Xu, Lei Shang, Jinxing Ye, Qi Qian, Yu-Feng Li, Baigui Sun, Hao Li, and Rong Jin. Dash: Semi-supervised learning with dynamic thresholding. In *ICML*, pages 11525–11536. PMLR, 2021. 2
- [68] Lihe Yang, Wei Zhuo, Lei Qi, Yinghuan Shi, and Yang Gao. St++: Make self-training work better for semi-supervised semantic segmentation. In *CVPR*, pages 4258–4267, 2022. 5, 6
- [69] Lihe Yang, Lei Qi, Litong Feng, Wayne Zhang, and Yinghuan Shi. Revisiting weak-to-strong consistency in semi-supervised semantic segmentation. In *CVPR*, pages 7236–7246, 2023. 2, 3, 5, 6, 13
- [70] Lihe Yang, Zhen Zhao, and Hengshuang Zhao. Unimatch v2: Pushing the limit of semi-supervised semantic segmentation. *IEEE TPAMI*, 2025. 2, 14
- [71] Sangdoon Yun, Dongyoon Han, Sanghyuk Chun, Seong Joon Oh, Youngjoon Yoo, and Junsuk Choe. Cutmix: Regularization strategy to train strong classifiers with localizable features. In *ICCV*, pages 6022–6031, 2019. 1, 13
- [72] Bowen Zhang, Yidong Wang, Wenxin Hou, Hao Wu, Jindong Wang, Manabu Okumura, and Takahiro Shinozaki. Flexmatch: Boosting semi-supervised learning with curriculum pseudo labeling. *NeurIPS*, 34:18408–18419, 2021. 2
- [73] Xiangyu Zhao, Zengxin Qi, Sheng Wang, Qian Wang, Xuehai Wu, Ying Mao, and Lichi Zhang. Rcps: Rectified contrastive pseudo supervision for semi-supervised medical image segmentation. *IEEE Journal of Biomedical and Health Informatics*, 2023. 1
- [74] Zhen Zhao, Lihe Yang, Sifan Long, Jimin Pi, Luping Zhou, and Jindong Wang. Augmentation matters: A simple-yet-effective approach to semi-supervised semantic segmentation. In *CVPR*, pages 11350–11359, 2023. 5, 6
- [75] Barret Zoph, Golnaz Ghiasi, Tsung-Yi Lin, Yin Cui, Hanxiao Liu, Ekin Dogus Cubuk, and Quoc Le. Rethinking pre-training and self-training. *NeurIPS*, 33:3833–3845, 2020. 2
- [76] Yuliang Zou, Zizhao Zhang, Han Zhang, Chun-Liang Li, Xiao Bian, Jia-Bin Huang, and Tomas Pfister. Pseudoseg: Designing pseudo labels for semantic segmentation. In *ICLR*, 2020. 5, 6

When Confidence Fails: Revisiting Pseudo-Label Selection in Semi-supervised Semantic Segmentation

Supplementary Material

A. Overview

In the supplementary material for CSL, we provide a proof of Eq. (8) (Sec.B), give a low-complexity implementation of CSL and pseudo-code (Sec.C), extend the implementation details and experimental comparison (Sec.D), supplements the analysis of residual dispersion (Sec.E), discuss the potential limitations (Sec.F), and gives more visual results (Sec.G).

B. Proof of Equation 8

For the pseudo-label selection problem in semi-supervised semantic segmentation, it can be formulated as:

$$\max_S \text{Tr}(S^T \Phi^T \Phi S), \text{ s.t. } S \in \{0, 1\}^{HW \times 2},$$

where S is the binary selection matrix subject to $\sum_c S_{n,c} = 1$ with $c \in \{1, 2\}$ indicating class indices, and $\text{Tr}(\cdot)$ denotes the matrix trace. Each column of $\Phi = [\mathbf{h}_1, \mathbf{h}_2, \dots, \mathbf{h}_{HW}]$ represents the feature $\mathbf{h}_n \in \mathbb{R}^2$ of pixel n .

Proof. Without loss of generality, the essential goal of pseudo-label selection is to assign pixel classes via S such that the selected pseudo-labels are optimal under a certain metric:

$$\mathcal{L}(S) = \sum_{n=1}^{HW} \varphi(\mathbf{z}_n, S_{n,:}),$$

where $\varphi(\cdot, \cdot)$ is a function that measures the potential risk of assigning pixel n to a specific class, with \mathbf{z}_n representing the pixel's feature. Considering the potential natural separation exhibited in Fig. 1, we employ intra-class consistency as the metric, which measures the distance between the pixel feature vector $\mathbf{z}_n = \mathbf{h}_n$ and the mean feature vector μ_c of its assigned class c , which can be expressed as

$$\varphi(\mathbf{z}_n, S_{n,:}) = \sum_{c=1}^2 S_{n,c} \|\mathbf{h}_n(c) - \mu_c\|^2,$$

thus $\mathcal{L}(S)$ can be reformulated as

$$\mathcal{L}(S) = \|\Phi - S(S^T S)^{-1} S^T \Phi\|_F^2,$$

let $\mathbf{P} = S(S^T S)^{-1} S^T$, the $\mathcal{L}(S)$ simplifies to

$$\mathcal{L}(S) = \|\Phi - \mathbf{P}\Phi\|_F^2.$$

Using the Frobenius norm identity

$$\mathcal{L}(S) = \|\Phi\|_F^2 - 2 \text{Tr}(\Phi^T \mathbf{P}\Phi) + \|\mathbf{P}\Phi\|_F^2,$$

since $\mathbf{P}^2 = \mathbf{P}$ (idempotence of projection matrices), thus

$$\mathcal{L}(S) = \|\Phi\|_F^2 - \text{Tr}(\Phi^T \mathbf{P}\Phi).$$

Minimizing $\mathcal{L}(S)$ is equivalent to maximizing $\text{Tr}(\Phi^T \mathbf{P}\Phi)$. Substituting \mathbf{P} :

$$\text{Tr}(\Phi^T \mathbf{P}\Phi) = \text{Tr}(\Phi^T S(S^T S)^{-1} S^T \Phi),$$

for binary classification, $S^T S = \text{diag}(n_1, n_2)$, where n_1 and n_2 are the number of pixels in each class. Thus:

$$\text{Tr}(\Phi^T \mathbf{P}\Phi) = \text{Tr}(S^T \Phi \Phi^T S) \cdot (n_1^{-1} + n_2^{-1}),$$

ignoring the normalization constant, this reduces to:

$$\max_S \text{Tr}(S^T \Phi^T \Phi S).$$

C. Algorithm

C.1. Low-complexity Implementation of Prediction Convex Optimization Separation

In Eq. (9), we used the eigenvectors u_i of $\Phi^T \Phi$. However, obtaining u_i through $\Phi^T \Phi$ is computationally expensive, especially when $\Phi \in \mathbb{R}^{2 \times HW}$ has a large number of columns, where $HW \gg 2$. so we provide an efficient alternative with Singular Value Decomposition (SVD).

The SVD of Φ is given by:

$$\Phi = \mathbf{U}\mathbf{\Sigma}\mathbf{V}^T,$$

where $\mathbf{U} \in \mathbb{R}^{2 \times 2}$ and $\mathbf{V} \in \mathbb{R}^{HW \times HW}$ are orthogonal matrix, $\mathbf{\Sigma} \in \mathbb{R}^{2 \times HW}$ is a diagonal matrix containing the singular values σ_i .

Substituting the SVD of Φ ,

$$\Phi^T \Phi = (\mathbf{U}\mathbf{\Sigma}\mathbf{V}^T)^T (\mathbf{U}\mathbf{\Sigma}\mathbf{V}^T),$$

which simplifies to

$$\Phi^T \Phi = \mathbf{V}\mathbf{\Sigma}^T \mathbf{U}^T \mathbf{U}\mathbf{\Sigma}\mathbf{V}^T.$$

Using the orthogonality of \mathbf{U} ($\mathbf{U}^T \mathbf{U} = \mathbf{I}$),

$$\Phi^T \Phi = \mathbf{V}\mathbf{\Sigma}^T \mathbf{\Sigma}\mathbf{V}^T.$$

Let $\mathbf{\Lambda} = \mathbf{\Sigma}^T \mathbf{\Sigma} = \text{diag}(\sigma_1^2, \sigma_2^2)$, where σ_i^2 are the squared singular values. Then

$$\Phi^T \Phi = \mathbf{V}\mathbf{\Lambda}\mathbf{V}^T.$$

This shows that \mathbf{V} contains the eigenvectors of $\Phi^T\Phi$, Λ contains the eigenvalues of $\Phi^T\Phi$.

Computing the eigenvectors of $\Phi^T\Phi$ via direct eigen-decomposition requires explicitly forming $\Phi^T\Phi$, which has a cost of $\mathcal{O}(HW^2)$ for matrix multiplication and $\mathcal{O}(HW^3)$ for eigen-decomposition. In contrast, computing the SVD of Φ has a cost of $\mathcal{O}(HW^2)$.

C.2. Pseudocode for Optimization Separation

Algorithm 1 provides the pseudocode for Prediction Convex Optimization Separation. Using a convex optimization strategy based on confidence distribution, CSL effectively excludes a large number of high-confidence false predictions in pseudo-label selection to improve the performance in semi-supervised semantic segmentation tasks.

Algorithm 1 Pseudocode of Prediction Convex Optimization Separation in a PyTorch-like style.

```
# pmax: Pixel-level maximum confidence
# vn: Pixel-level residual dispersion
def PCOS(pmax, vn):
    # combine pmax and vn into a feature matrix  $\Phi$ 
     $\Phi$  = stack([pmax, vn], axis=1).T
    # extract the top two eigenvectors from  $\Phi$ 
    U, Sigma, VT = svd( $\Phi$ )
    eig_vectors = VT[:, :2]
    # constructing the optimal selection matrix
    S = argmax(abs(eig_vectors), axis=1)
    # calculate stats for each class
    stats = [( $\Phi$ [S == c].mean(dim=1),
               $\Phi$ [S == c].std(dim=1)) for c in range(2)]
    # select the reliable class
    mu, sigma = max(stats, key=lambda x:x[0])
    # smooth loss weight
    weight = exp(-(( $\Phi$ -mu)/(8*sigma))**2)
    weight = weight.prod(dim=0)
    # preserving reliable prediction weights
    weight[( $\Phi$ [0, :]>mu[0])|( $\Phi$ [1, :]>mu[1])] = 1
    return weight
```

C.3. Pseudocode for Trusted Mask Perturbation

In Sec. 3.4 of our paper, we propose the Trusted Mask Perturbation Strategy. The core idea of this method is to enhance the mutual information between low-confidence regions and pseudo-labels to strengthen the fitting of these regions. Specifically, we use high-confidence predictions from weakly augmented outputs as pseudo-labels but randomly discard their image content, while the image content of low-confidence predictions is entirely preserved. This forces the network to infer the classes of high-confidence regions based on the image content of low-confidence regions, thereby compensating for the underfitting in low-confidence areas. To clarify things, we present the pseudocode of the threshold updating strategy in a PyTorch-like style.

Algorithm 2 Pseudocode of Trusted Mask Perturbation in a PyTorch-like style.

```
# x.w: Image with weak augmentation perturbation
# image_size: The length or width of the image
# block_size: The masking patch size
# masking_rate: The masking pixel ratio
# f: segmentation network

pred_w = f(x.w)
mask_w = pred_w.argmax(dim=1).detach()
# compute weights using PCOS on the projection
weight = PCOS(Projection(pred_w))
# create a reliability mask
reli_mask = (weight == 1)
# gain patch-based perturbation mask (Eq. (12))
mask_size = img_size // block_size
cover_mask = (rand(mask_size, mask_size) <
              masking_rate).float()
cover_mask = interpolate(cover_mask,
                        size=img_size, mode='nearest')
# perturbation only for reliable predictions
cover_mask = cover_mask & reli_mask
# constructing perturbed images
x_m = x.s.clone()
x_m[cover_mask == 1] = 0
pred_m = f(x_m)
# calculated loss
criterion = CrossEntropyLoss()
loss_m = criterion(pred_m, mask_w)
```

D. Extensive Experiment Details and Results

D.1. More Implementation Details

Following prior works [34, 69], we employ random scaling between [0.5, 2.0], cropping, and flipping as weak augmentations. We combine ColorJitter, random grayscale, Gaussian blur, and CutMix [71] for strong augmentations. Weak augmentations and a modified strong augmentation (without random grayscale and Gaussian blur) are applied before Trusted Mask Perturbation. Additionally, we incorporate 50% random channel dropout as feature perturbations to encourage robust feature representations as in previous works [50, 51, 69]. For computational efficiency, mixed-precision training based on BrainFloat16 is utilized.

D.2. More Experimental Results

Different loss weights. In Tab. 7, we investigate the impact of different loss weightings on segmentation accuracy. The imbalance between consistency loss and masking loss significantly affects model performance. Moreover, assigning excessively high or low loss weights to the unlabeled data also leads to a degradation in performance. The results indicate that the optimal performance is achieved when $[\lambda_1, \lambda_2]$ are set to [0.5, 0.5].

A: We conducted experiments comparing threshold-based methods and CSL on identical model predictions. As shown in Tab. 9, CSL achieves consistent accuracy improvements (+4.1%), while maintaining competitive recall (+1.0%).

λ_1	λ_2	1/16(92)	1/8(183)	1/2(732)
0.50	0.50	76.8	79.6	80.9
0.75	0.25	75.6	78.1	79.7
0.25	0.75	75.2	77.6	79.2
0.30	0.30	76.3	79.1	80.2
0.70	0.70	75.7	78.4	79.8
1.00	1.00	72.5	76.6	77.6

Table 7. Impact of different loss weights, evaluated on the original PASCAL VOC 2012 with a crop size of 321.

Method	1/16	1/8	1/4	1/2	Full
CSL	76.8	79.6	80.3	80.9	82.3
Class-specific CSL	74.6	78.3	79.1	79.7	80.6

Table 8. Comparison of CSL and class-specific strategy, evaluated on the original PASCAL VOC 2012 with a crop size of 321.

Metrics		plane	bicyc	bus	car	chair	perso	sofa	mean
Sampling	Base	96.2	93.1	98.0	93.2	82.0	91.0	78.6	91.0
Accuracy		90.8	75.4	90.1	85.4	33.4	83.7	50.2	82.4
Recall		96.6	97.6	93.2	89.5	81.8	87.5	86.7	93.6
Sampling	CSL	92.3	85.7	94.1	89.5	63.1	85.6	71.2	87.6
Accuracy		95.1	82.4	96.4	91.7	42.5	89.1	60.4	86.5
Recall		97.1	98.2	95.8	92.3	80.1	87.7	94.5	94.6

Table 9. Pseudo-Label sampling rate, accuracy and recall comparison under PASCAL original 1/4 Splits with class-wise metrics.

Class-specific prediction selection. In semi-supervised semantic segmentation, due to the long-tailed distribution of datasets, the confidence distributions of predictions vary significantly across classes. This suggests that employing a class-specific convex optimization strategy could potentially yield performance gains. To analyze this, we reconstruct the feature matrix Φ into class-specific feature spaces for Prediction Convex Optimization Separation:

$$\Phi_k = \{h_n \mid h_n \in \Phi, k_n^* = k\} \quad (16)$$

where Φ_c is Class-specific feature matrix for class k and k_n^* is the predicted class label for pixel n .

We conducted ablation experiments presented in Tab. 8, where it can be observed that using class-specific schemes results in significant performance degradation. This may be attributed to the fact that most classes have too few pixel samples within instances to maintain an effective convex optimization strategy.

Augmentations of Trusted Mask Perturbations. In Tab. 11, we evaluate the impact of various augmentations on Trusted Mask Perturbations. Adding CutMix leads to significant performance degradation, as it introduces misleading contextual information by directly stitching image

dataset	92	183	366	732	1464
D_l	73.2	77.1	78.8	79.4	80.3
D_u	76.8	79.6	80.3	80.9	82.3
$D_l \cup D_u$	75.6	78.4	79.6	80.1	81.7

Table 10. Ablation study of masking datasets under 1/2 splits. For the labeled dataset, predictions are treated as reliable predictions.

Method	1/8	1/2
A^ω only	78.3	79.1
$A^\omega \& A^s$	78.7	79.5
$A^\omega \& A^s$ W/O Cutmix	79.1	79.8
$A^\omega \& A^s$ W/O grayscale	79.0	80.4
$A^\omega \& A^s$ W/O (Cutmix & grayscale)	79.6	80.9

Table 11. Comparison of augmentations strategies for TMP, evaluated on the original PASCAL VOC 2012 with a crop size of 321.

Method	Encoder	1/16	1/8	1/4	1/2	full
UniMatchV2	DINOv2	79.0	85.5	85.9	86.7	87.8
Ours	DINOv2	80.2	85.8	86.3	87.4	88.1
AllSpark	SegFormer	76.1	78.4	79.8	80.8	82.1
Ours	SegFormer	77.4	80.2	81.5	83.5	85.3

Table 12. Influence of different network architectures, evaluated on the original PASCAL VOC 2012 with a crop size of 513.

patches while the trusted masking mechanism forces the model to learn contextual relationships, resulting in negative effects. Similarly, random grayscale enhances the sample by reducing color diversity, which conflicts with the masking mechanism and results in substantial information loss. Therefore, we adopt enhancements that exclude CutMix and random grayscale as additional Augmentations to the masking strategy.

Selection of Masking Datasets. To evaluate the impact of applying the mask perturbation to different subsets: labeled images, unlabelled images, and the combination of both, experiments were performed under different splits, as detailed in Tab. 10. Results show applying masking to labeled data or the combination leads to progressively severe performance degradation as the number of labeled data samples decreases. This phenomenon can be attributed to the network learning contextual relationships present only in the labeled data instances and applying them to unlabeled data. **Different network Architectures.** Considering that different encoders may exhibit varying degrees of overconfidence in their representations and utilize contextual relationships through distinct mechanisms, we supplement additional experiments with diverse network architectures in Tab. 12. Specifically, DINOv2-S adopts the hyperparameters from Unimatchv2 [70], while SegFormer-B5[54] shares

v_n	$H(p_n)$	H_{res}	m_n	1/8	1/4
✓				79.6	80.3
✓	✓			77.3	78.5
✓		✓		77.5	79.1
✓			✓	76.9	78.2
✓	✓	✓	✓	71.5	76.3

Table 13. Comparison of different combinations of metrics, evaluated on the original PASCAL VOC 2012 with a crop size of 321.

the training configuration described in Sec. 4.1. Experimental results reveal that our Confidence-aware Structure Learning (CSL) achieves consistent performance improvements across architectures, demonstrating its effectiveness as an architecture-independent framework.

E. More Analysis for residual dispersion

E.1. Why residual dispersion but not other common metrics

The choice of residual dispersion as a reliability metric stems from its theoretical foundation in entropy minimization principles. As derived in Eq. (4)-Eq. (7), the cross-entropy objective naturally decomposes into two complementary terms: the maximum confidence $p_n(k')$ and residual dispersion v_n . This decomposition reveals an intrinsic geometric relationship, that reliable predictions must simultaneously maximize confidence in the dominant class and dispersion among residual probabilities.

Traditional metrics like entropy $H(p_n)$ and prediction margin m_n fail to meet this criterion. Though entropy theoretically encourages unimodal distributions, it inadvertently tolerates pathological multi-peaked configurations. Consider predictions $p_A = [0.5, 0.5, 0, \dots, 0]$ and $p_B = [0.5, 0.01, \dots, 0.01]$. Paradoxically, p_A exhibits lower entropy despite being less reliable. This demonstrates entropy inability to distinguish valid unimodal predictions from problematic multi-modal ones.

Residual entropy $H_{res} = -\sum_{k \neq k'} p_n(k) \log p_n(k)$ avoid such problem and is ostensibly similar to the second term in Eq. (4), but its additional linear dependence on $p_n(k)$ significantly reduces its ability to judge prediction credibility under overconfidence.

Margin $m_n = p_n(k') - \max_{k \neq k'} p_n(k)$ focuses only on the top two categories. In the case of overconfidence, the margin is completely dominated by the maximum confidence and shows no discrimination.

E.2. Why not use multiple metrics

While combining multiple metrics theoretically enhances pseudo-label selection with negligible additional time overhead, considering that metrics like entropy or margin are re-

peated measurements of Eq. (4), adding such redundant features will introduce covariance conflicts that will degrade the model performance. As shown in Tab. 13, optimal performance is achieved when only maximum confidence and residual dispersion are considered.

F. Potential Limitations

In CSL, we employ a convex optimization strategy within the confidence distribution feature space to exclude potential high-confidence erroneous pseudo-labels caused by model overconfidence. However, we observe that when the proportion of labeled data is extremely small, the significant disparity in the marginal distributions between sample sets leads to unavoidable cognitive bias. This limitation is particularly pronounced in real-world scenarios, where such imbalanced data splits are common. Thus, an important avenue for future research could involve leveraging limited labeled data more effectively to calibrate cognitive biases and improve the quality of pseudo-labels.

Additionally, although the theoretical validity of residual dispersion is established under the general principles of semi-supervised semantic segmentation, given the broad applicability of entropy minimization, this proof can be readily extended to similar domains such as semi-supervised classification or unsupervised domain adaptation. Similarly, introducing direct confidence calibration methods commonly used in other fields into semi-supervised semantic segmentation represents another promising technical pathway. We leave these potential extensions for future exploration.

Last but not least, CSL utilizes the masking of reliable regions to leverage contextual relationships, thereby enhancing the model’s learning in low-confidence areas. However, we find that as the interfering information surrounding low-confidence regions is masked, predictions in these areas tend to be more accurate compared to unmasked regions. Yet, due to the potential for errors, the information from these areas is discarded during training. Therefore, a potential approach could be to further screen this valid information. This could potentially complement the direct supervision signals for low-confidence regions, fostering a more effective learning process.

G. More Visualizations

In Fig. 8, we show that the method in this paper and other methods More segmentation results on the PASCAL VOC 2012 dataset.

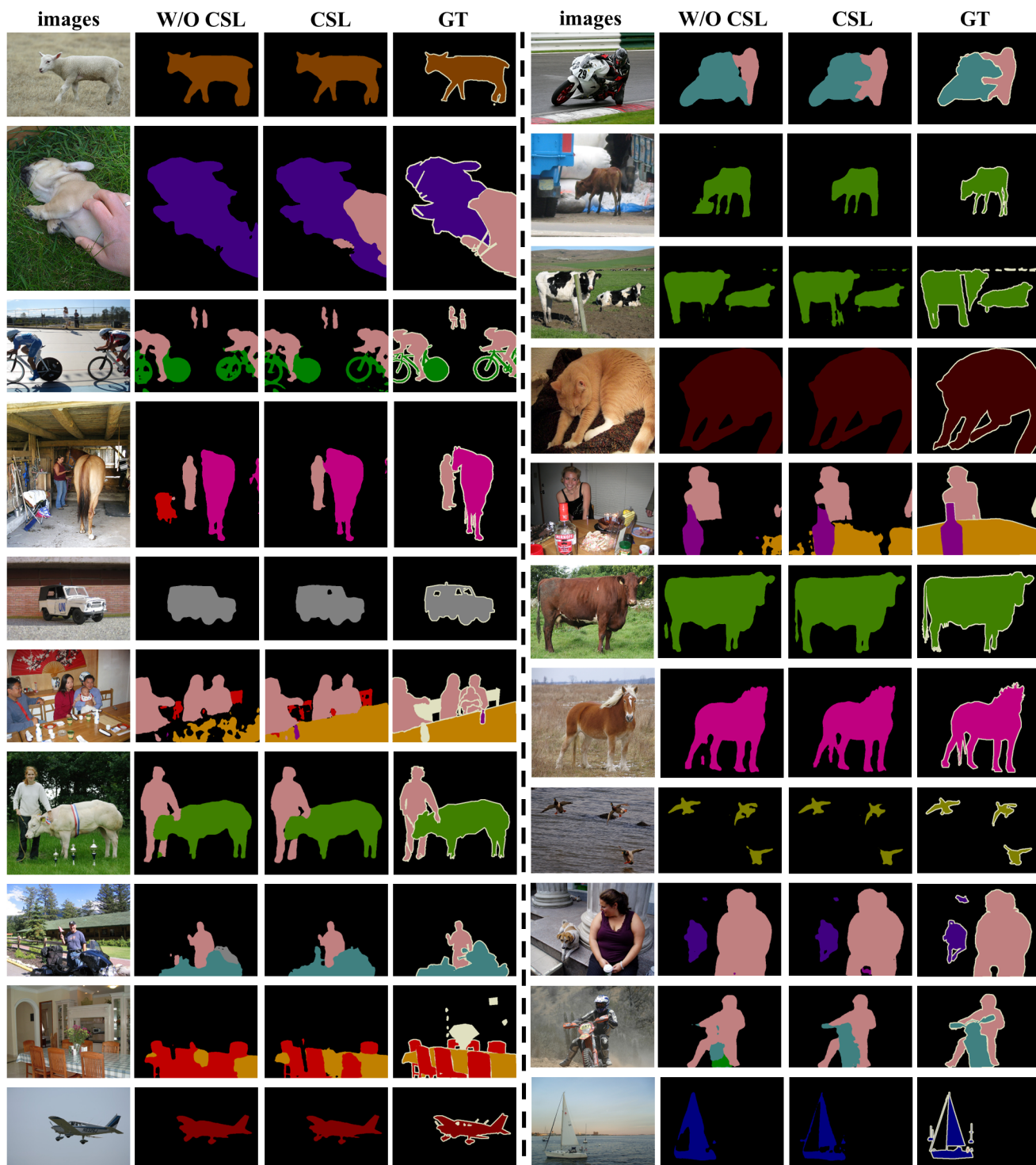


Figure 8. More visualization of the segmentation results on the PASCAL VOC 2012 dataset on 1/8 splits with a crop size of 513.